Kinetics and Catalysis, Vol. 45, No. 1, 2004, pp. 122–132. Translated from Kinetika i Kataliz, Vol. 45, No. 1, 2004, pp. 134–145.

Reactions of Adsorbed CH_3 Radicals and the Products of Their Decomposition at Mo and Cu Surfaces According to Spatially Resolved TPR Data

M. U. Kislyuk and V. V. Savkin

Semenov Institute of Chemical Physics, Russian Academy of Sciences, Moscow, 119991 Russia

Received November 28, 2002

Abstract—Reactions in the layer of CH_3 radicals adsorbed on the surfaces of polycrystalline molybdenum and copper were studied using the method of temperature-programmed reaction (TPR). After N_2 and $CH_3^{\bullet}$ adsorption (the products of azomethane pyrolysis) on molybdenum, N_2, H_2, and CH_4 were observed in comparable amounts in the TPR spectrum. At the same time, only methane was detected in the TPR products on the copper surface. The spatial distributions of CH_4 desorption flows were measured, which were indicative of translational excitation of these molecules. The direct measurements of the rates of the CH_4 molecules desorbed from the copper surface showed that their translational energy was 10–15 times greater than the thermal one. The mechanisms of reactions on the Mo and Cu surfaces are proposed. The rate constants were calculated for some of the elementary steps.

In recent years, experimental data suggesting that many reactions of oxidative catalysis occur through the formation and consecutive transformations of free radicals were obtained [1–3].

In some processes of catalytic methane oxidation, the methyl radical is a primary species of methane activation in catalytic oxidation [4, 5]. The overall rate of the reaction and the selectivity to various products depend on the kinetics of heterogeneous reactions of the methyl radical and other intermediates formed after $CH_3^{\bullet}$ adsorption. A study of the adsorption of $CH_3^{\bullet}$ radicals and their subsequent transformations on surfaces is of great interest. So far these reactions have been studied on clean and oxidized Pt(111) [6], Ni(100), Ni(111) [7, 8], polycrystalline Mo [9], and Mo(100) [10] surfaces.

In this work, we study the reactions of CH_3 radicals on the surfaces of polycrystalline molybdenum and copper by the TPR method. These metals differ substantially in their adsorption and catalytic properties. Molybdenum is capable of adsorbing many molecules (including nitrogen) with their dissociation. In contrast, copper displays a low activity in dissociative adsorption. Thus, the activation energy of hydrogen dissociation on copper is rather high [11]. Therefore, we may expect a considerable difference in the behavior of these systems.

EXPERIMENTAL

Experiments were performed in an ultrahigh vacuum setup (with a maximal pressure of residual gases of 5×10^{-10} Torr) described previously [9, 12]. The setup was equipped with an omegatron mass spectrometer, an Auger electron spectrometer, and a system for gas supply in the form of an effusive molecular beam.

Samples with the size $10 \times 4 \times 0.05$ mm were made of molybdenum (99.99%) or copper (99.99%) foil. A sample was placed at the center of a vacuum chamber on a manipulator, which allowed us to turn the sample 360° so that its front surface was exposed to either the molecular beam of the gas studied, or the electron beam of the Auger spectrometer. The front surface of a sample can also be oriented through the inlet window of a mass spectrometer at various angles. The temperature of a sample was measured using W–Re (for molybdenum) or Chromel–Alumel (for copper) thermocouples welded on the rear side of the sample. Immediately before runs, the samples were carefully degassed and freed of carbon admixtures by the procedure described previously [9, 12]. No other admixtures were detected on the samples under study. Cleaning was repeated after each experimental series consisting of 10–15 runs.

Methyl radicals were produced by pyrolysis of azomethane ($CH_3N{=}NCH_3$) in a quartz capillary heated to 1100 K. This capillary was also used to form the effusive beam of radicals or other gases directed at the front of a sample, which was held at room temperature. In every run the $CH_3^{\bullet}$ radicals were adsorbed until saturation.

Upon adsorption, a sample placed in various positions was heated in a programmed mode at a ramp of 30–40 K/s. During this process, the rates of desorption of products of surface reactions and the spatial distribu-

0023-1584/04/4501-0122 © 2004 MAIK “Nauka / Interperiodica”

tions of desorption flows were recorded using an omegatron mass spectrometer. The average rates of desorbed methane molecules were also measured in the course of TPR on the copper surface.

RESULTS AND DISCUSSION

TPR Spectra

In addition to methyl radicals and nitrogen molecules, the flow of azomethane pyrolysis products ($CH_3N{=}NCH_3$) contains the admixtures of methane, ethane, and molecular hydrogen [10]. No adsorption of methane and ethane on the molybdenum or copper surfaces was experimentally observed under similar conditions (room temperature, exposure at 10^{-6} Torr for 20 min). Adsorption of nitrogen and hydrogen at the copper surface was not detected either.

$CH_3^{\bullet}$/Mo. Figure 1 shows a typical TPR spectrum obtained after the adsorption of azomethane pyrolysis products on the sample forming a saturation coverage corresponding (as we suppose) to the monolayer coverage. Figure 1 shows that comparable amounts of nitrogen, hydrogen, and methane are desorbed from the surface. The corresponding temperatures (T_{max}) of the TPR peak maximums are 1200, 1000, and 870 K, respectively.

We performed the experiments on recombinative temperature-programmed desorption (TPD) of individual gases (nitrogen and hydrogen), which were previously adsorbed on the surface of molybdenum samples.

The activation energies (E) and the corresponding preexponential factors (k^0) of the rate constants of desorption were evaluated by the formulas [13]:

$$\ln(F/\ln F) = [rT_1T_2\ln(\theta_1/\theta_2)]/[T_{max}(T_2 - T_1)], \quad (1)$$

$$E = RT_{max}\ln(F/\ln F), \quad (2)$$

where $F = (k^0\theta_{max}^{r-1}T_{max})/b$; T_1 and T_2 are the temperatures at which the rate of desorption is equal to half the maximum rate; θ_{max}, θ_1, and θ_2 are the values of the surface coverage at T_{max}, T_1, and T_2, respectively; $r = 2$ is the kinetic order of desorption; b is the rate of heating equal to 30–40 K/s.

Assuming second-order desorption, the value of $\ln(\theta_1/\theta_2)$ is 1.6 [13].

Because the dimensionless values of the surface coverage were used as concentrations, all rate constants had the same dimension (s^{-1}).

The calculated activation energies (E, kJ/mol) of hydrogen and nitrogen desorption are equal to 160 ± 10 and 270 ± 15, respectively; the corresponding preexponential factors ($\log k^0$, s^{-1}) are equal to 13.6 ± 1.0 and 12.5 ± 1.5, respectively.

The above parameters of the rate constants of hydrogen and nitrogen desorption agree well with the published data [14–17]. This coincidence supports a dissociative character of adsorption of these gases on the molybdenum surface.

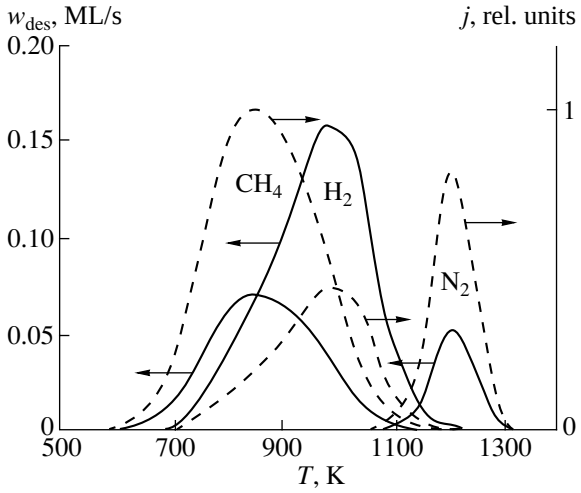

Fig. 1. TPR spectrum observed after monolayer adsorption of the products of azomethane pyrolysis (N_2 and $CH_3^{\bullet}$) on the molybdenum surface: the experimental dependences of ion currents (j) corresponding to H_2^+, N_2^+, and CH_4^+ (dotted lines); the absolute rates of desorption (w_{des}), the calculation of which is described in [9] (solid lines); the rate of heating is 37 K/s.

Note that the peak in the TPD spectrum obtained after individual adsorption of N_2 on the molybdenum surface practically coincides with the TPD peak of nitrogen observed after the simultaneous adsorption of N_2 and $CH_3^{\bullet}$. In the second case, the parameters of the rate constant of nitrogen desorption calculated by Eqs. (1) and (2) are equal to $E = 280 \pm 15$ kJ/mol and $\log k^0 = 13.5 \pm 1.5$. Within the experimental error, these values agree well with the parameters given above.

On the other hand, the TPR spectrum of hydrogen produced by adsorbed methyl radicals differs substantially from the TPD spectra that are observed after adsorption of molecular hydrogen. These spectra differ in the shape of the peak form (dragged-out front) and in the value of T_{max} (Fig. 2).

$CH_3^{\bullet}$/Cu. Analogous experiments on TPR were performed with the monolayers of methyl radicals adsorbed on copper. As distinct from molybdenum, only methane having $T_{max} = 480$ K and a considerable high-temperature tail was detected in the TPR spectra on copper (Fig. 3).

Mechanisms of the Methane Formation

It is remarkable that ethane formation is not observed in the studied process on either molybdenum or copper, i.e., no recombination of adsorbed CH_3 radicals occurs. Steric hindrances apparently arise when

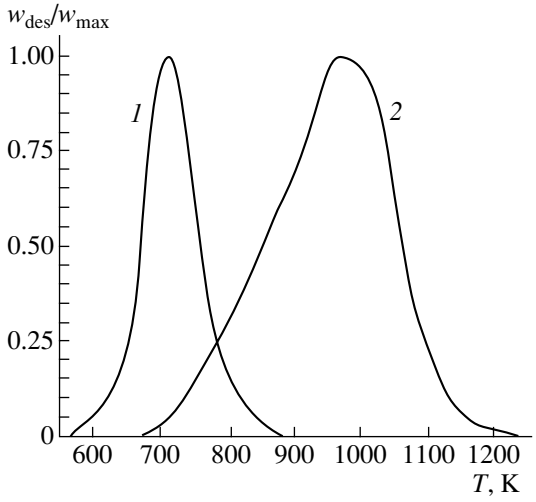

Fig. 2. TPD/TPR spectra (*1*) of hydrogen previously adsorbed at the molybdenum surface and (*2*) of the decomposition product of adsorbed methyl radicals.

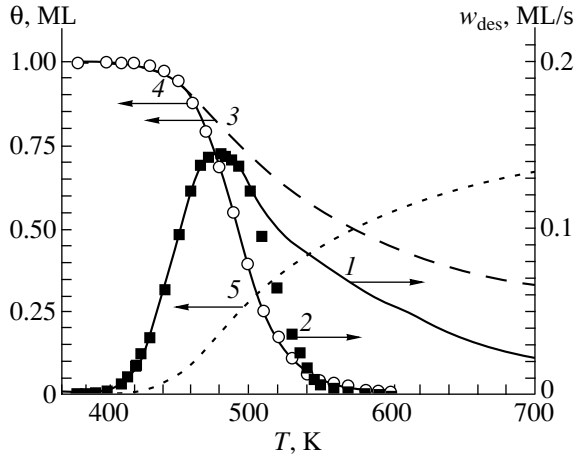

Fig. 3. (*1*) TPR spectrum of methane observed after monolayer adsorption of $CH_3^{\bullet}$ at the copper surface and the temperature dependences calculated from the spectrum of (*2*) the $0.5\,w_{CH_3}$ value corresponding to the $k_1^{(II)}$ constant, (*3*) θ_Σ, (*4*) θ_{CH_3}, and (*5*) the integral $\int_0^t w_{CH_4} dt$.

the carbon atoms of two methyl groups approach each other.

$CH_3^{\bullet}$/Mo. The absence of nitrogen-containing compounds other than N_2 in the TPR spectra obtained on the molybdenum samples testifies that adsorbed nitrogen atoms solely recombine with one another and do not react with methyl radicals and the products of their decomposition. Note that N_2 is desorbed at high temperatures when other reagents excluding carbon atoms are completely desorbed from the sample. Thus, adsorbed nitrogen influences the reactions of adsorbed methyl radicals and the products of their decomposition on the molybdenum surface by sole blocking a part of the active sites on the surface.

Based on the above results, we proposed scheme (I) for the reaction in the mixed layer, containing N atoms and $CH_3^{\bullet}$ radicals adsorbed on molybdenum [9]:

$$\begin{aligned}
&(1)\ [CH_3] \rightleftharpoons [CH_2] + [H],\\
&(2)\ [CH_2] \rightleftharpoons [CH] + [H],\\
&(3)\ [CH] \rightleftharpoons [C] + [H],\\
&(4)\ 2[N] \longrightarrow N_2,\\
&(5)\ 2[H] \longrightarrow H_2,\\
&(6)\ [CH_3] + [H] \longrightarrow CH_4,\\
&(7)\ [C] \longrightarrow \{C\}.
\end{aligned} \qquad \text{(I)}$$

In this scheme, gaseous products are presented without brackets, adsorbed compounds are given in brackets, and carbon dissolved in the metal is shown in braces.

Steps (1)–(3) in scheme (I) are considered reversible based on estimates presented below. The energies of the C–H bond in the adsorbed fragments (CH_3, CH_2, and CH) appear to be close to those in the hydrocarbons (CH_4, C_2H_4, and C_2H_2, respectively), i.e., equal to 425–473 kJ/mol [18]. The energy of the H–surface bond (q) was evaluated using the E value and the dissociation energy of the hydrogen molecule (D) from the relation

$$q = (E + D)/2, \qquad (3)$$

assuming that the activation energy of dissociative adsorption of hydrogen on molybdenum is zero, i.e., the E value coincided with the heat of adsorption. The substitution of E and D values into Eq. (3) gives: $q = 300 \pm 15$ kJ/mol. Thus, forward reactions (1)–(3) are endothermic; therefore reverse reactions (1)–(3) are possible.

$CH_3^{\bullet}$/Cu. The mechanism of methane formation from methyl radicals adsorbed on copper fundamentally differs from that on molybdenum. The absence of hydrogen in the TPR spectra suggests that there is no dissociation of the adsorbed CH_3, CH_2, and CH. The reason for that is that the binding energy (q) of an adsorbed hydrogen atom with the copper surface (220 kJ/mol) [19] is substantially lower than that in the case of the molybdenum surface, whereas the energies of the C–H bond dissociation in hydrocarbons are 425–473 kJ/mol [18]. The formation of methane and other transformations proceed through disproportionation (scheme II):

$$\begin{aligned}
&(1)\ 2[CH_3] \longrightarrow CH_4 + [CH_2],\\
&(2)\ [CH_3] + [CH_2] \longrightarrow CH_4 + [CH],\\
&(3)\ [CH_3] + [CH] \longrightarrow CH_4 + [C],\\
&(4)\ 2[CH_2] \rightleftharpoons [CH_3] + [CH],
\end{aligned} \qquad \text{(II)}$$

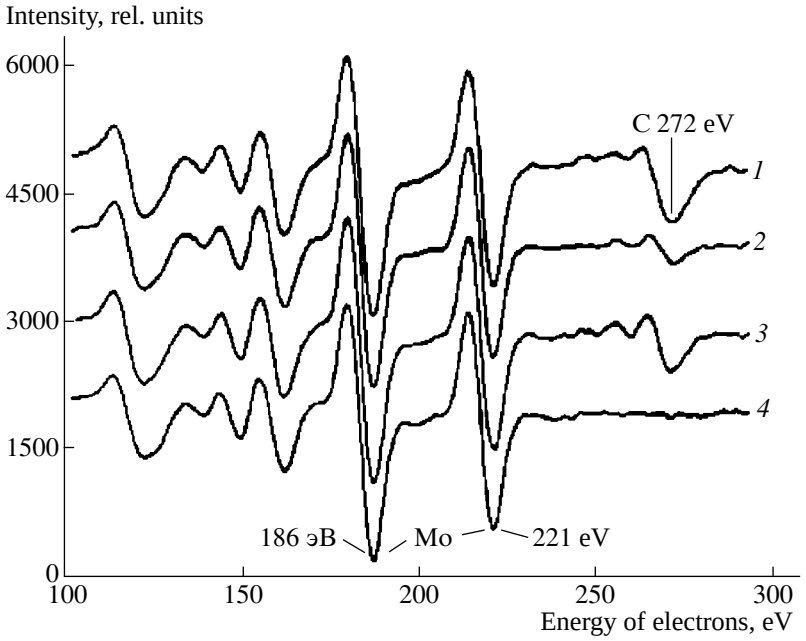

Fig. 4. Auger spectra of the surface of the molybdenum sample: (*1*) after adsorption of ethylene at room temperature, (*2*) after programmed heating of the sample with adsorbed ethylene in a vacuum at a temperature of 1100 K and subsequent cooling to room temperature, (*3*) after 20 analogous cycles (adsorption–heating–cooling), (*4*) a procedure similar to (*2*) but with heating to 1300 K.

$$(5)\ [CH_2] + [CH] \rightleftharpoons [CH_3] + [C],$$

$$(6)\ 2[CH] \rightleftharpoons [CH_2] + [C].$$

Reactions (4)–(6) in scheme (II) are presented as reversible, because the differences in the values of the C–H bond energy in the above-mentioned adsorbed fragments appear to be small, and the heat effects of these reactions are insignificant.

The material balance with respect to carbon for the reactions described by schemes (I) and (II) can be written as

$$N_{[CH_3]} = N_{CH_4} + N_{[C]} + N_{\{C\}}. \quad (4)$$

Here, $N_{[CH_3]}$ is the initial amount of methyl radicals adsorbed on the sample surface; N_{CH_4}, $N_{[C]}$, and $N_{\{C\}}$ are the amounts of the methane molecules formed, adsorbed, and absorbed carbon atoms, respectively, at the end of the run. Even though no hydrogen is formed in the reaction (as it is observed on copper), the total amount of carbon atoms ($N_{[C]} + N_{\{C\}}$) remaining on the sample after programmed heating equals 25% of the initial amount of adsorbed methyl radicals. For molybdenum samples, this value should be higher.

Although carbon is formed in every run in the amount of at least 25% of a monolayer (ML), the TPR spectra are reproducible in a series involving 10–15 runs (Figs. 1, 3). If the sample surface is covered to a great extent with carbon atoms or surface carbide, adsorption properties of the samples (particularly, their ability to dissociate nitrogen on molybdenum) should change continuously. However, we did not experimentally observe such a phenomenon.

The strong dissociative adsorption of nitrogen on the molybdenum samples suggests that their surface is mostly composed of pure molybdenum and is not covered with carbon or molybdenum carbide.

It is likely that in the course of our experiments we deal with the stationary surface, which on heating to 1300 K is freed of carbon, because carbon transfers to the bulk with the formation of a solid solution of carbon in molybdenum.

To check this assumption, we studied the Auger spectra of the molybdenum surface after several cycles of ethylene adsorption–desorption with heating the sample to various temperatures (Fig. 4). Ethylene was chosen as a model system for the following reasons. A considerable amount of nitrogen is adsorbed on the surface in the course of adsorption of azomethane pyrolysis products on molybdenum. On the other hand, ethylene easily dissociates on molybdenum to give CH_2 groups, which decompose and produces gaseous methane and adsorbed carbon on further heating. As can be seen from Fig. 4, on heating the sample containing adsorbed ethylene to a temperature of 1100 K, carbon is accumulated on the surface in much smaller amounts than those suggested by the stoichiometry of the reaction $C_2H_4 \longrightarrow CH_4 + C$. This fact indicates that the main portion of carbon formed dissolves in the molybdenum bulk under these conditions. On heating the sample to 1300 K (the conditions of our TPR measurements), no Auger signal of carbon is detected. Taking into account that the outgoing Auger electrons are

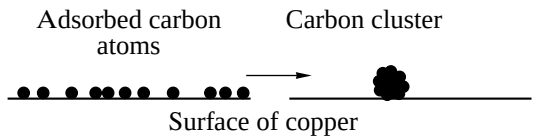

Fig. 5. Formation of carbon clusters from the C atoms adsorbed on the copper surface.

localized near the metal surface (10–20 Å in thickness), we can understand why the adsorption–catalytic properties of the sample are not changed in the course of several cycles of measurements. We also performed the runs with samples that were treated as follows: adsorption–heating to 1300 K–cooling (20 cycles). After heating these samples to high temperatures (1600–1700 K), only the line corresponding to carbon was observed in the Auger spectra of the surface. Consequently, at rather high temperatures, surface segregation of carbon occurs to form a multilayer graphite coating on the surface. In this case, surface cleaning requires heating the sample at 1700 K and an oxygen pressure of 10^{-6} Torr for several hundred hours.

Another mechanism for the removal of carbon from the surface is effective on copper. As distinct from other metals, copper does not form solid solutions of carbon. Copper carbides are unstable and decompose with explosion [20]. We assume that due to low adhesion of carbon with the copper surface, the adsorbed carbon atoms (arising in the course of the reaction) become mobile at high temperatures and assemble together in dense clusters as shown in Fig. 5. Indirect evidence for this assumption was obtained in the calculation of the $k_6^{(II)}$ constant in scheme (II) (see below).

Calculation of the Rate Constants of the Elementary Steps

The TPR spectra of hydrogen and methane (Figs. 1, 3) cannot be processed using Eqs. (1) and (2), because both H_2 and CH_4 are the products of multiple-step processes rather than of desorption, and this is shown in Fig. 2. We quantitatively described these spectra based on schemes (I) and (II).

The partial pressure of a gas in a vacuum system where the gas is desorbed and evacuated is described by the equation [21]:

$$V(\mathrm{d}P/\mathrm{d}t) = w_{\mathrm{des}} - sP, \tag{5}$$

where V is the volume of a vacuum chamber, t is the time, w_{des} is the rate of desorption, and s is the evacuation rate.

Under our experimental conditions, the s values were equal to 100, 50, and 40 l/s for hydrogen, methane and nitrogen, respectively. At such high values of evacuation rate, the left side of Eq. (5) may be neglected, and we have

$$w_{\mathrm{des}} = sP. \tag{6}$$

For the copper surface, where only methane is desorbed and the initial concentration of methyl radicals is considered corresponding to the monolayer, the TPR spectra are normalized using Eq. (4), which under these conditions takes the form

$$\theta^0_{\mathrm{CH_3}} = 1 = \int_0^\infty w_{\mathrm{CH_4}}\mathrm{d}t + 0.25. \tag{7}$$

Here, $\theta^0_{\mathrm{CH_3}}$ is the initial surface coverage by methyl radicals.

The absolute values of w_{des} (ML/s) for H_2, CH_4, and N_2 ($w_{\mathrm{H_2}}$, $w_{\mathrm{CH_4}}$, and $w_{\mathrm{N_2}}$) on molybdenum were obtained from the balance equations with respect to hydrogen and nitrogen:

$$\theta^\circ_{\mathrm{CH_3}} = \left(4\int_0^\infty w_{\mathrm{CH_4}}\mathrm{d}t + 2\int_0^\infty w_{\mathrm{H_2}}\mathrm{d}t\right)/3, \tag{8}$$

$$\theta^\circ_{\mathrm{N}} = 2\int_0^\infty w_{N_2}\mathrm{d}t. \tag{9}$$

Provided that the surface is initially completely filled with adsorbed methyl radicals and nitrogen atoms, we obtain:

$$\theta^0_{\mathrm{CH_3}} + \theta^0_{\mathrm{N}} = 1. \tag{10}$$

Equations (8)–(10) contain the values of initial surface coverages by methyl radicals ($\theta^0_{\mathrm{CH_3}}$) and nitrogen atoms (θ^0_{N}). In these equations, we did not take into account the surface coverage by hydrogen (θ^0_{H}), although hydrogen was detected in the molecular beam of the products of azomethane pyrolysis [10]. However, it was shown previously [9] that the initial concentration of hydrogen on the molybdenum surface was negligibly small.

TPR spectra shown by dotted lines in Fig. 1 were converted into the absolute rates of desorption (ML/s) of the gases studied (the solid lines) using Eqs. (8)–(10) with the method described in [9]. Thus, the TPR spectra were normalized and the values of the initial surface coverage were determined: $\theta^0_{\mathrm{CH_3}} = 0.87$ and $\theta^0_{\mathrm{N}} = 0.13$. The difference observed in the initial surface concentrations of these species upon their adsorption from the beam, in which the concentration of nitrogen atoms is higher than that of the methyl radicals [2, 10], is determined by the difference in their sticking coefficients at room temperature. Thus, the probability of sticking the

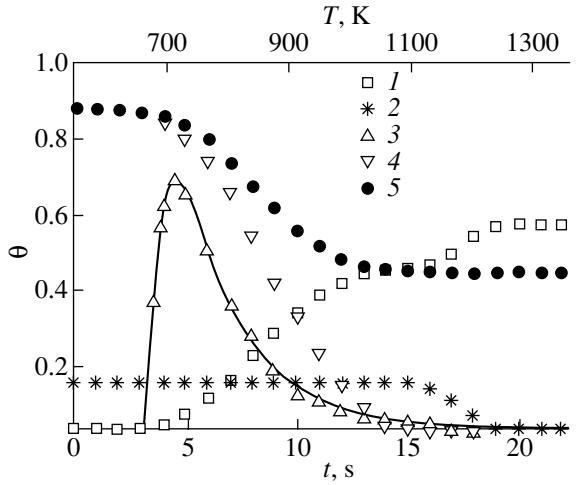

Fig. 6. Dependences of the surface concentrations (*1*) θ, (*2*) θ_N, (*3*), 100 θ_H, (*4*) θ_{CH_3}, and (*5*) $\theta_\Sigma = \theta_{CH_3} + \theta_{CH_2} = \theta_{CH} + \theta_C$ on the time (temperature) obtained in [9] on the molybdenum samples.

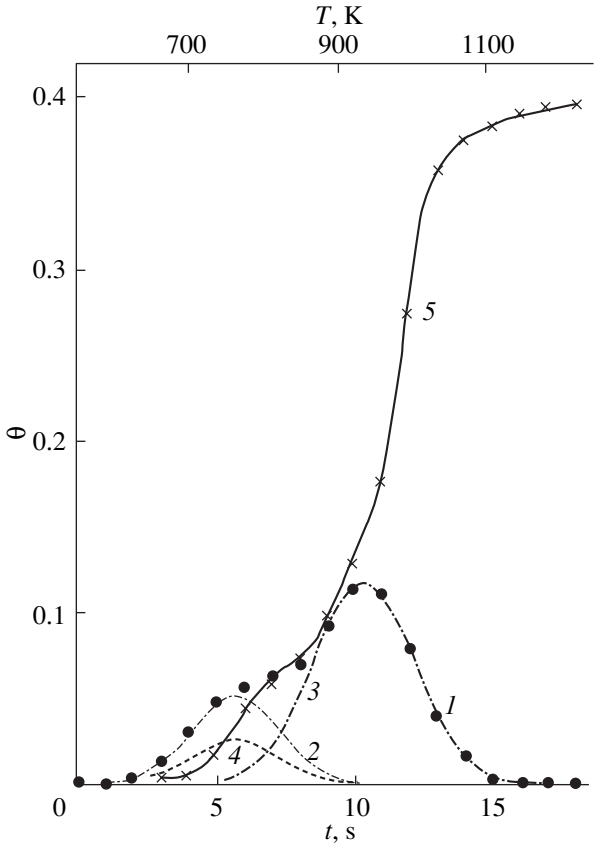

Fig. 7. Dependence of (*1*) ($2\theta_{CH_2} + \theta_{CH}$) on the time (temperature) calculated in [9] for the molybdenum samples its decomposition into two peaks (*2*) $2\theta_{CH_2}$ and (*3*) θ_{CH}, as well as the dependence of (*4*) θ_{CH_2} and (*5*) θ_C.

radicals is essentially higher than that of the dissociative adsorption of nitrogen.

Henceforth we will use the following designations: θ_H, θ_N, θ_{CH_3}, θ_{CH_2}, θ_{CH}, θ_C, and θ, which stand for the values of the actual surface coverage by hydrogen and nitrogen atoms, carbon-containing species (CH_3, CH_2, CH, and C), and fraction of the free surface, respectively; θ_C means the total amount of carbon (both surface and dissolved in the bulk of a metal) produced in one run; $k_i^{(I)}$, $k_i^{(II)}$, $k_{-i}^{(I)}$, and $k_{-i}^{(II)}$ are the rate constants of the *i*th forward and reverse reactions in schemes (I) and (II).

$CH_3^\bullet$/Mo. To determine the rate constants of individual steps in scheme (I), we processed the TPR spectra (Fig. 1) [9]. In this work, we present only several important results.

Figures 6 and 7 show the dependences of θ, θ_{CH_3}, θ_{CH_2}, θ_{CH}, θ_C, θ_N, θ_H, and $\theta_\Sigma = \theta_{CH_3} + \theta_{CH_2} + \theta_{CH} + \theta_C$ on the time (temperature), which was calculated from TPR spectra in [9].

Note that carbon started to accumulate on the surface when the CH groups were not formed in an appreciable amount. In addition, as can be seen from the plot $\theta_C(t)$, the rate of carbon formation sharply increases when CH groups appear on the surface.

The results of the calculations allow us to assume that in addition to the reactions involved in scheme (I), carbon formation directly from the CH_2 groups should be taken into account:

$$(2^*)\ [CH_2] \longrightarrow [C] + 2[H].$$

The rate constant of reaction (2*) is denoted by $k^*_2{}^{(I)}$.

Figure 8 shows the Arrhenius plots of the obtained rate constants corresponding to scheme (I). Table 1 presents the values of preexponential factors and the activation energies for these constants.

A characteristic inflection in the curve for $k_2^{(I)} + k^*_2{}^{(I)}$ (Fig. 8, curve *3*) allowed us to describe this dependence by the sum of two Arrhenius functions.

We assigned one of these functions, which was characterized by a low preexponential factor and an activation energy close to zero, to $k^*_2{}^{(I)}$ because this function mainly contributed to the above sum at low temperatures. This allows us to explain the formation of surface carbon bypassing the CH species.

Thus, the second function describes the $k_2^{(I)}$ constant and is characterized by the standard preexponential factor and a high activation energy (Table 1).

We determined the $k_3^{(I)}$ constant over the high temperature region, where we could neglect the term

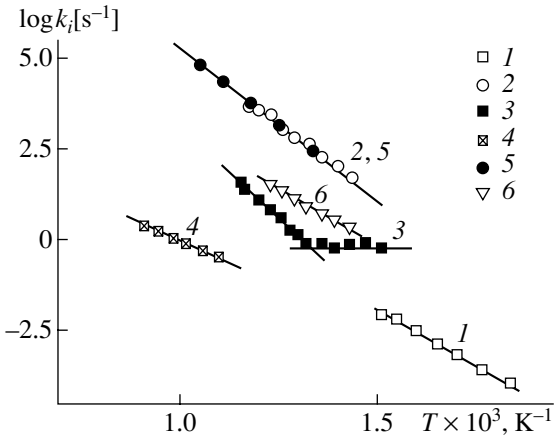

Fig. 8. Temperature dependences of the rate constants of the steps of scheme (I) obtained by analysis of the experimental TPR spectra (Fig. 1): (*1*) $k_1^{(I)}$, (*2*) $k_1^{(I)}$, (*3*) $k_2^{(I)} + k_2^{*(I)}$, (*4*) $k_{3eff}^{(I)}$, (*5*) $k_5^{(I)}$, and (*6*) $k_6^{(I)}$.

$k^{*(I)}_2\theta_{CH_2}$. We did not take into account the reverse reactions as well. The obtained effective constant $k_{3eff}^{(I)}$ is adequately described by the Arrhenius equation (Fig. 8).

The constants obtained by analysis of scheme (I) are presented in Table 1 and in Fig. 8 (as the temperature dependences).

Note that all constants are calculated in terms of the homogeneous surface model and are adequately described by the Arrhenius equation.

Data presented in Fig. 8 show that the rate constants of self-recombination of hydrogen atoms ($k_5^{(I)}$) coincide with those of recombination of hydrogen atoms with the CH_2 groups ($k_{-1}^{(I)}$) over a wide range of temperatures. The reason is that the rate-determining factor for both processes is the mobility of adsorbed hydrogen.

On the other hand, the rate constant of recombination of hydrogen with the adsorbed CH_3 groups ($k_6^{(I)}$) is 20–30 times lower than the $k_5^{(I)}$ and $k_{-1}^{(I)}$ values over the same temperature interval. In this case, the rate-determining factor appears to be the recombination act, because it is associated with steric hindrances (this shows itself as a somewhat low preexponential factor in the $k_6^{(I)}$ constant).

The low preexponential factor of the effective constant $k_{3eff}^{(I)}$, which describes the decomposition of the surface CH_2 groups with the carbon formation, is probably due to the fact that the above constant is not elementary. Thus, the reverse reaction and the diffusion of carbon into the bulk of metal can occur simultaneously.

In a quasi-steady-state approximation with respect to the surface carbon concentration, the value of $k_{3eff}^{(I)}$ can be presented as:

$$k_{3eff}^{(I)} = k_3^{(I)}k_7^{(I)}/(k_7^{(I)} + k_{-3}^{(I)}\theta_H). \quad (11)$$

It is possible that a change in the relation between the terms in the denominator of Eq. (11) with increasing temperature leads to a low value of the effective preexponential factor.

Table 1. Parameters of the rate constants of the steps in scheme (I)

Reaction	$k_i^{(I)}$	k^0, s^{-1}	E, kJ/mol	T, K
$[CH_3] \longrightarrow [CH_2] + [H]$	$k_1^{(I)}$	$1.1 \times 10^{7 \pm 1}$	115 ± 4	550–670
$[CH_2] + [H] \longrightarrow [CH_3]$	$k_{-1}^{(I)}$	$1.1 \times 10^{13 \pm 1}$	151 ± 4	660–900
$[CH_2] \longrightarrow [CH] + [H]$	$k_2^{(I)}$	$2.0 \times 10^{14 \pm 2}$	210 ± 10	740–860
$[CH_2] \longrightarrow [C] + 2[H]$	$k_2^{*(I)}$	0.7 ± 0.3	0 ± 5	660–760
$[CH] \longrightarrow [C] + [H]$	$k_{3eff}^{(I)}$	$6.0 \times 10^{5 \pm 1}$	90 ± 5	900–1100
$2[N] \longrightarrow N_2$	$k_4^{(I)}$	$3.0 \times 10^{13.0 \pm 1.5}$	280 ± 15	1000–1300
$2[H] \longrightarrow H_2$	$k_5^{(I)}$	$4.0 \times 10^{13 \pm 2}$	160 ± 10	750–950
$[CH_3] + [H] \longrightarrow CH_4$	$k_6^{(I)}$	$1.3 \times 10^{9 \pm 1}$	117 ± 6	700–830

Based on the analysis of experimental data, we infer that direct decomposition of the CH_2 groups into carbon (bypassing the step of CH formation) is possible.

Note that at temperatures below 600 K, the CH_3 groups and the products of their decomposition (the CH_2 and CH groups) adsorbed on the molybdenum surface are stable. CH_2 groups have the least stability and decompose to give CH, H, and carbon and recombine with the adsorbed hydrogen atoms to produce methyl groups.

$CH_3^{\bullet}$/Cu. When analyzing the TPR spectrum of methane (Fig. 3), we calculated the total surface coverage with carbon-containing species $\theta_\Sigma = \theta_{CH_3} + \theta_{CH_2} + \theta_{CH} + \theta_C$ from the balanced equation with respect to carbon:

$$\theta_\Sigma = 1 - \int_0^t w_{CH_4} dt. \quad (12)$$

The dependences of θ_Σ, w_{CH_4}, and the integral from Eq. (12) on the time (temperature) are shown in Fig. 3.

Then, we determined the rate constant $k_1^{(II)}$ which characterized the rate of disproportionation of the CH_3 radicals in scheme (II). It was assumed that it is this process that dominates the initial stage. In this case the expression for the rate of the $CH_3^{\bullet}$ radical consumption (w_{CH_3}) can be written as

$$w_{CH_3} = -d\theta_{CH_3}/dt = 2k_1^{(II)}(\theta_{CH_3})^2 = 2w_{CH_4}. \quad (13)$$

Upon integrating (13), we have

$$\theta_{CH_3} = 1 - 2\int_0^t w_{CH_4} dt. \quad (14)$$

Eventually, we obtain the equation for the calculation of $k_1^{(II)}$, depending on w_{CH_4} only:

$$k_1^{(II)} = w_{CH_4} \Big/ \left(1 - 2\int_0^t w_{CH_4} dt\right)^2. \quad (15)$$

Figure 9 shows the temperature dependence of this constant, which is described by the Arrhenius equation with the following parameters: $k^0 = 10^{12.0 \pm 0.5}$ s^{-1}, $E = 110 \pm 5$ kJ/mol.

Figure 3 presents the temperature dependence of the $0.5 w_{CH_3}$ value, corresponding to the $k_1^{(II)}$ constant. Figure 3 shows that this dependence coincides very closely with the experimental curve of the rate of methane desorption (w_{CH_4}) over a wide range of temperatures, including a maximum of the TPR peak. Using the $k_1^{(II)}$ constant, we determined the values of the surface coverage by CH_3 radicals (θ_{CH_3}) up to 600 K, when the calculated θ_{CH_3} value was close to zero. The results of the calculations are also shown in Fig. 3.

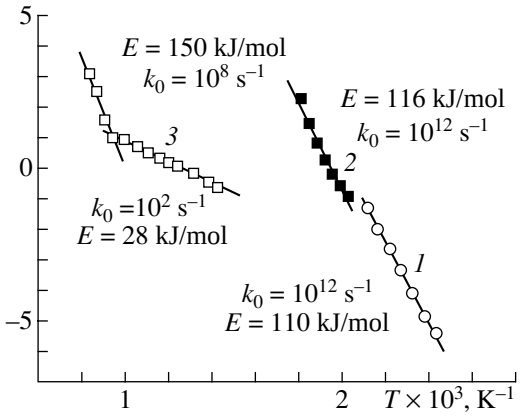

Fig. 9. Temperature dependences of the rate constants of the steps of scheme (II) obtained by analysis of the experimental TPR spectra (Fig. 3): (*1*) $k_1^{(II)}$, (*2*) $k_2^{(II)}$, and (*3*) $k_6^{(II)}$.

In the temperature range from 350 to 500 K, the above dependence is rather precise, because the rate of methane desorption is consistent with the rate of the consumption of adsorbed CH_3 radicals.

In the temperature interval 500–600 K, the calculation of the θ_{CH_3} value appears to be less precise, because reactions (2)–(6) in scheme (II) involving the CH_2 and CH groups begin to play a decisive role. However, these processes result both in the consumption of CH_3 groups and their formation (i.e., compensate for each other). In this connection, we assumed that the actual curve of methyl radical consumption differs insignificantly from the dependence calculated from the $k_1^{(II)}$ constant describing the bimolecular disproportionation of methyl radicals (Fig. 3).

To determine the θ_{CH_2} and θ_{CH} values at temperatures of 350–600 K, we used the balanced equation with respect to hydrogen and carbon:

$$3\theta_{CH_3} + 2\theta_{CH_2} + \theta_{CH} = 3\theta_{CH_3}^0 - 4\int_0^t w_{CH_4} dt, \quad (16)$$

$$\theta_{CH_3} + \theta_{CH_2} + \theta_{CH} + \theta_C = \theta_{CH_3}^0 - \int_0^t w_{CH_4} dt. \quad (17)$$

Provided that $\theta_{CH_3}^0 = 1$ and ignoring the θ_C value, we obtained from these equations the expressions for θ_{CH_2}

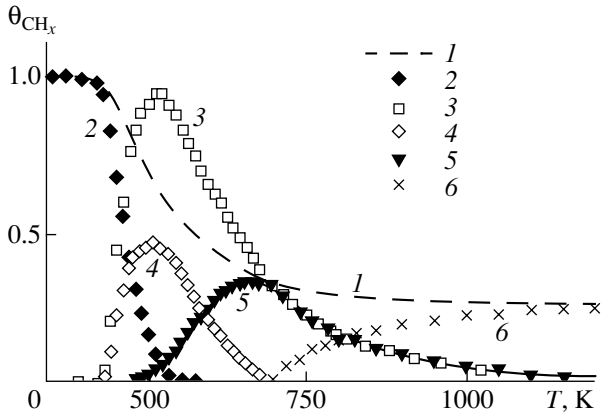

Fig. 10. Dependences of the surface concentrations (*1*) $\theta_\Sigma = \theta_{CH_3} + \theta_{CH_2} + \theta_{CH} + \theta_C$, (*2*) θ_{CH_3}, (*3*) $2\theta_{CH_2} + \theta_{CH}$, (*4*) θ_{CH_2}, (*5*) θ_{CH}, and (*6*) θ_C on the time (temperature) obtained for the copper samples by analysis of scheme (II).

and θ_{CH}:

$$\theta_{CH_2} = 2(1 - \theta_{CH_3}) - 3\int_0^t w_{CH_4} dt, \quad (18)$$

$$\theta_{CH} = 2\int_0^t w_{CH_4} dt - (1 - \theta_{CH_3}). \quad (19)$$

The results of these calculations are shown in Fig. 10 and allow us to evaluate the rate constant $k_2^{(II)}$, the temperature dependence of which is presented in Fig. 9. We estimated the $k_2^{(II)}$ value by the equation

$$d\theta_{CH}/dt = k_2^{(II)}\theta_{CH_3}\theta_{CH_2}, \quad (20)$$

in which $d\theta_{CH}/dt$ was determined by approximating the $\theta_{CH}(t)$ relation by a smooth function. In the above calculation, steps (3)–(6) of scheme (II) are not taken into account, which results in a small deviation of the obtained temperature dependence from the linear one in the coordinates of the Arrhenius equation. The value of $k_2^{(II)}$ is somewhat lower than that of $k_1^{(II)}$ due to a higher activation energy (Table 2).

When calculating the values of the surface coverage at high temperatures (700–1200 K), we ignored the θ_{CH_2} and θ_{CH_3} terms in Eqs. (16) and (17). This approach allowed us to determine the temperature dependences of θ_{CH} and θ_C over the above-mentioned temperature range:

$$\theta_{CH} = 3 - 4\int_0^t w_{CH_4} dt, \quad (21)$$

$$\theta_C = -2 + 3\int_0^t w_{CH_4} dt. \quad (22)$$

The obtained dependences of θ_{CH} and θ_C on the temperature (time) are shown in Fig. 10. The temperature dependence of $(2\theta_{CH_2} + \theta_{CH})$, calculated by Eq. (16) (the balance with respect to hydrogen) is also presented in Fig. 10. This curve and the plot of the function $\theta_\Sigma = f(T)$ intersect at $T \approx 700$ K. Evidently, near 700 K, carbon begins to accumulate in detectable amounts on the surface in accordance with the above assumptions for solving Eqs. (18), (19), (21), and (22).

The obtained data on the θ_{CH} and θ_C values in the temperature range from 700 to 1200 K allowed us to determine the effective rate constant $k_6^{(II)}$ by the equation

$$d\theta_C/dt = k_6^{(II)}\theta_{CH}^2, \quad (23)$$

in which the $d\theta_C/dt$ value was determined upon the approximation of the $\theta_C(t)$ relation by a smooth function.

The temperature dependence of this constant in the coordinates of the Arrhenius equation has an inflection point at a temperature of ~1000 K (Fig. 9). The effective values of the activation energy and the preexponential factor at $T < 1000$ K are equal to 28 kJ/mol and 10^2 s^{-1}, respectively. At $T > 1000$ K, the activation energy increases to 150 kJ/mol, and the preexponential

Table 2. Parameters of the rate constants of the steps in scheme (II)

Reaction	$k_i^{(II)}$	k^0, s^{-1}	E, kJ/mol	T, K
$2[CH_3] \longrightarrow [CH_2] + CH_4$	$k_1^{(II)}$	$1 \times 10^{12 \pm 1}$	110 ± 4	400–490
$[CH_3] + [CH_2] \longrightarrow [CH] + CH_4$	$k_2^{(II)}$	$1 \times 10^{12 \pm 2}$	116 ± 8	500–600
$2[CH] \longrightarrow [CH_2] + [C]$	$k_3^{(II)}$	$1 \times 10^{8 \pm 2}$	150 ± 10	1050–1200

factor equals 10^8 s^{-1}. This effect can be due to the following facts. The reverse reaction $[CH_2] + [C] \longrightarrow 2[CH]$ plays a crucial role at temperatures below 1000 K. At $T > 1000$ K, carbon atoms begin to aggregate to form clusters (Fig. 5), and the reverse reaction is suppressed. Therefore, the true value of the $k_6^{(II)}$ constant is determined at the high-temperature portion of the curve (Table 2).

Dynamics of Methane Desorption

In 1968, Van Willigen observed the distributions of desorbed hydrogen molecules diffusing through plane metallic membranes that were sharply directed along the normal to the surface [22]. He proposed a model based on the concept of microscopic reversibility, which explained the revealed phenomenon by excitation of the translational degree of freedom of the molecules along the normal to the surface [22]. This report gave impetus to studies on the dynamics of desorption.

It was previously suggested that desorbed molecules have the temperature of the surface. The sharply directed spatial distributions of the desorption flow (SDDF) of molecules allow one to consider that these molecules have excess translational energy, i.e., the molecules are repelled from the surface in the course of desorption. This concept was confirmed for the first time by the direct measurements of the rates of hydrogen molecules [23] and then by the results obtained for other systems in various laboratories [24].

Based on the principle of microscopic reversibility, the following equation was derived in the above study [22]:

$$I/I_0 = [(\varepsilon\cos^2\varphi)\exp(-\varepsilon\tan^2\varphi)]/[(\varepsilon + 1)\cos\varphi]. \quad (24)$$

Here, I_0 and I are the intensities of the desorption flow directed along the normal to the sample surface and at a φ angle to the surface, respectively; $\varepsilon = E_a/kT_s$, where E_a is the activation energy of adsorption, k is the Boltzmann constant, and T_s is the temperature of the surface.

Note that at $\varepsilon = 0$, Eq. (24) transforms into the known Knudsen equation

$$I/I_0 = \cos\varphi, \quad (25)$$

which is valid for evaporation and non-activated adsorption.

To describe the observed SDDF, the simple empirical equation

$$I/I_0 = \cos^n\varphi, \quad (26)$$

is used, which is a rather exact approximation of Eq. (24), particularly at high n values. A simple relation exists between the n and ε values [25]:

$$n \approx 2\varepsilon + 1. \quad (27)$$

The results of the measurements of SDDF of methane formed on copper and molybdenum are shown in Fig. 11. As can be seen from Fig. 11, the desorption flows of methane are concentrated along the normal to the sample surface and are described by empirical Eq. (26), the distribution on copper being considerably sharper. The values of the n and ε parameters are equal to 16 ± 2 and 8 ± 1 (for copper), 6.3 ± 0.5 and 2.7 ± 0.3 (for molybdenum), respectively.

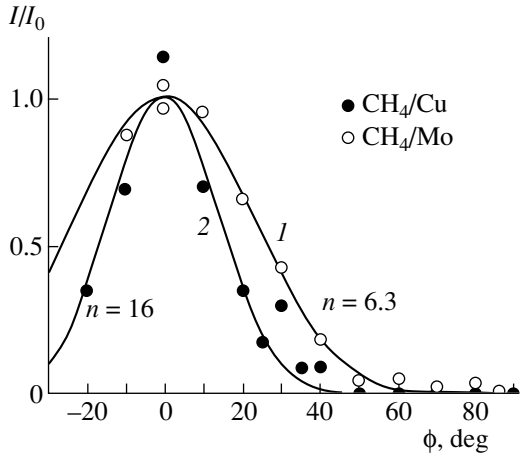

Fig. 11. Spatial distributions of the desorption flow of methane arising from the reactions of the methyl radicals adsorbed on the surface of (*1*) molybdenum and (*2*) copper.

An estimation of the activation energy of dissociative adsorption using ε and T_{max} gives the values 32 ± 5 and 19 ± 3 kJ/mol for copper and molybdenum, respectively. As noted in [24], this estimate can be too low because of the roughness of the surface of a polycrystalline sample.

The average rate of the methane molecules desorbed from the copper surface $\langle v \rangle$ was measured in [12] and equal to 2400 ± 500 m/s. The translational temperature (T_{trans}) and the activation energy of adsorption (E_a) were calculated by the formulas [25]:

$$T_{trans} = (\langle v \rangle^2\pi\mu)/(2R), \quad (28)$$

$$E_a = (R/\pi)(\sqrt{T_{trans}} - \sqrt{T_s})^2, \quad (29)$$

where μ is the molecular weight of methane, R is the universal gas constant, and T_s is the temperature of the surface (480 K).

The value $E_a = 34 \pm 16$ kJ/mol was found. Within the limits of experimental error this value coincides with that obtained from analysis of SDDF of methane (32 ± 5 kJ/mol).

Thus, it was shown by the two methods that the excited molecules of methane, the translational temperature of which was 10–15 times higher than that of the surface, were desorbed from the copper surface under the above conditions.

We did not measure the rates of methane molecules desorbed from molybdenum. However, we can evaluate the T_{trans} value, using the correlation between the SDDF parameters and the translational energy (temperature)

of the desorbed molecules [24]. This calculation showed that the T_{trans} value for molybdenum was 1.5–2 times lower than that for the copper samples, although the temperature of the molybdenum surface at which the measurements were performed was twice as high as that for copper.

Thus, the results obtained show that the mechanism of methyl radical decomposition on copper differs substantially from that on molybdenum. On molybdenum, the consecutive dissociation of CH_x groups and the reverse recombination reactions occur. Hydrogen, methane, and carbon are the final products. In the case of copper, no hydrogen was detected in the gaseous products, which can be explained by the occurrence of the surface reactions by the mechanism of the disproportionation of CH_x groups. Note that for both metals the results are reproducible in a series, involving 10–15 cycles of the consecutive TPR measurements, although each of these cycles produce carbon in amounts of 0.25 ML. These facts suggest that the surface of the samples remains free of carbon for the most part. However, the mechanisms of surface cleaning are different for the metals studied. Carbon dissolves in the bulk of molybdenum, whereas carbon clusters are formed on copper at high temperatures. The dynamics of desorption of the reaction product (methane) is noticeably different for the two metals as well. On copper, the spatial distributions of the methane desorption flow are essentially sharper than those on molybdenum.

ACKNOWLEDGMENTS

This work was supported by the Russian Foundation for Basic Research, project nos. 99-03-32114a and 02-03-33097.

REFERENCES

1. Driscoll, D.J., Campbell, K.D., and Lunsford, J.H., *Adv. Catal.*, 1987, vol. 35, p. 139.
2. Garibyan T.A., Margolis L.Ya., *Catal. Rev. – Sci. Eng.*, 1989–1990, vol. 31, p. 35.
3. Sinev, M.Yu., Margolis, L.Ya., and Korchak, V.N., *Usp. Khim.*, 1995, vol. 64, no. 4, p. 373.
4. Nersessyan, L.A., Vardanyan, I.A., Kegeyan, E.M., Margolis, L.Ya., and Nalbandyan, A.B., *Dokl. Akad. Nauk SSSR*, 1975, vol. 220, no. 3, p. 605.
5. Driscoll, D.J., Martir, W., Wang, J.-X., and Lunsford, J.H., *J. Am. Chem. Soc.*, 1985, vol. 107, no. 6, p. 5062.
6. Fairbrother, D.H., Peng, X.-D., Stair, P.C., *et al., Symp. on Methane and Alkane Conversion Chemistry, 207th National ACS Meeting*, San Diego: Am. Chem. Soc., 1994, p. 280.
7. Hall, R.B., Castro, M., Kim, C.-M., *et al., Symp. on Methane and Alkane Conversion Chemistry, 207th National ACS Meeting*, San Diego: Am. Chem. Soc., 1994, p. 282.
8. Yang, Q.Y. and Ceyer, S.T., *J. Vac. Sci. Technol. A*, 1988, vol. 6, no. 3, p. 851.
9. Kislyuk, M.U., Tret'yakov, I.I., Savkin, V.V., and Sinev, M.Yu., *Kinet. Katal.*, 2000, vol. 41, no. 1, p. 71.
10. Smudde, G.H., Jr., Min, Yu., and Stair, P.C., *J. Am. Chem. Soc.*, 1993, vol. 115, no. 3, p. 1988.
11. Kislyuk, M.U. and Tret'yakov, I.I., *Kinet. Katal.*, 1972, vol. 18, no. 3, p. 657.
12. Kislyuk, M.U., Savkin, V.V., and Tret'yakov, I.I., *Kinet. Katal.*, 2001, vol. 42, no. 4, p. 594.
13. Kislyuk, M.U., Sklyarov, A.V., and Dangyan, T.M., *Izv. Akad. Nauk SSSR, Ser. Khim.*, 1975, no. 10, p. 2161.
14. Cerny, S., Ponec, V., and Hladek, L., *J. Catal.*, 1966, vol. 5, no. 1, p. 27.
15. Mahning, M. and Schmidt, L.D., *Z. Phys. Chem.*, 1971, vol. 75, p. 227.
16. Lapyonlade, J. and Neil, K.S., *C. R. Acad. Sci., Ser. C*, 1972, vol. 274, no. 3, p. 2125.
17. Ko, S.M. and Schmidt, L.D., *Surf. Sci.*, 1974, vol. 42, no. 3, p. 508.
18. *Kratkii spravochnik fiziko-khimicheskikh velichin* (Concise Handbook of Physicochemical Quantities), Mishchenko, K.P. and Ravdel', A.A., Eds., Leningrad: Khimiya, 1972, p. 172.
19. Ehrlich, G., *J. Chem. Phys.*, 1959, vol. 31, no. 4, p. 1111.
20. Cotton, F. and Wilkinson, J., *Advanced Inorganic Chemistry: A Comprehensive Text*, New York: Wiley, 1965, vol. 2, p. 130.
21. Dushman, S., *Scientific Foundations of Vacuum Technique*, Lafferty, J.M., Ed., New York: Willey, 1962, p. 715.
22. Van Willigen, W., *Phys. Lett. A*, 1968, vol. 28, no. 2, p. 80.
23. Dabiri, A.E., Lee, T.J., and Stickney, R.E., *Surf. Sci.*, 1971, vol. 26, no. 2, p. 522.
24. Kislyuk, M.U., *Kinet. Katal.*, 2002, vol. 43, no. 5, p. 645.
25. Savkin, V.V. and Kislyuk, M.U., *Kinet. Katal.*, 1996, vol. 37, no. 4, p. 591.
26. Savkin, V.V. and Kislyuk, M.U., *Kinet. Katal.*, 1997, vol. 38, no. 5, p. 793.